Inducing a finite in-plane piezoelectricity in graphene with low concentration of inversion symmetry-breaking defects

Published version:

DOI:10.1021/acs.jpcc.5b01471

Inducing a Finite In-plane Piezoelectricity in Graphene with Low Concentration of Inversion Symmetry-breaking Defects

Kh. E. El-Kelany,[*,†] Ph. Carbonnière,[†] A. Erba,[¶] and M. Rérat[†]

Equipe de Chimie Physique, IPREM UMR5254, Université de Pau et des Pays de l'Adour, 64000 Pau, France, Chemistry Department, Faculty of Science, Minia University, Minia 61519, Egypt, and Dipartimento di Chimica and Centre of Excellence NIS (Nanostructured Interfaces and Surfaces), Università di Torino, via Giuria 5, IT-10125 Torino (Italy)

E-mail: khaled.el-kelany@univ-pau.fr

Abstract

We show that a finite in-plane piezoelectricity can be induced in graphene by breaking its inversion center with any in-plane defect, in the limit of vanishing defect concentration. We first consider different patterns of BN-doped graphene sheets of D_{3h} symmetry, whose electronic and piezoelectric (dominated by the electronic rather than nuclear term) properties are characterized at the *ab initio* level of theory. We then consider other in-plane defects, such as holes of D_{3h} or C_{2v} point-symmetry, and confirm that a common limit value (for low defect concentration) of the piezoelectric response of graphene is obtained regardless of the particular chemical or physical nature of the defects ($e_{11} \approx 4.5 \times 10^{-10}$ C/m and $d_{11} \approx 1.5$ pm/V for direct and

[*]To whom correspondence should be addressed

[†]Equipe de Chimie Physique, IPREM UMR5254, Université de Pau et des Pays de l'Adour, 64000 Pau, France

[‡]Chemistry Department, Faculty of Science, Minia University, Minia 61519, Egypt

[¶]Dipartimento di Chimica and Centre of Excellence NIS (Nanostructured Interfaces and Surfaces), Università di Torino, via Giuria 5, IT-10125 Torino (Italy)

converse piezoelectricity, respectively). This in-plane piezoelectric response of graphene is one-order of magnitude larger than the out-of-plane previously investigated one.

1 Introduction

In the continuous quest for the fabrication of nanoelectromechanical systems (NEMS) and nanoscale devices, a great attention has been devoted in recent years to low-dimensional materials due to their peculiar, highly-tunable, physico-chemical properties.[1–3] A variety of NEMS devices has been successfully produced (nanosized switches, sensors, motors, energy harvesters, actuators, etc.)[4–7] which essentially rely on quantum-size effects.[8] Most of such devices require some sort of dynamical control of atomic displacements and nanoscale deformations. In this respect, piezoelectricity turns out to be an extremely useful property in that it allows for fine-tuning the induced nano-strain by modulating an applied electric field (or *vice versa*). Among other low-dimensional systems, such as nanoparticles, nanotubes, nanoribbons and fullerenes, graphene-based[9] materials have been playing a paramount role in the fabrication of innovative devices for electronics, optoelectronics, photonics and spintronics,[10–16] due to the many extraordinary properties of the 2D carbon allotrope: high electron-mobility, hardness and flexibility, anomalous quantum-hall effect, zero band gap semi-metallic character, etc.[17–19]

Graphene lacks any intrinsic piezoelectricity due to its symmetry inversion center. The induction of piezoelectricity into graphene sheets would lead to a new branch of possible applications in NEMS devices requiring high electromechanical coupling. A recent theoretical study has highlighted the possibility of engineering piezoelectricity in graphene by adsorbing light atoms (such as H, Li, K, F) on one side of its surface; a rather small out-of-plane piezoelectric response has been reported.[20] Apart from atom adsorption, other techniques can be used to break the inversion symmetry of graphene sheets, such as hole formation,[21] stacking control in graphene bilayers,[22] application of non-homogeneous strain,[23] and chemical doping.[24–26] Among these strategies, chemical doping seems the most promising as it already represents an effective experimental mean for tuning structural and electronic properties (such as band gap and work function) of graphene.[24,25,27–29]

Boron nitride (BN) chemical doping of graphene has recently been successfully achieved in different configurations and concentrations: semiconducting atomic layers of hybrid *h*-BN and graphene domains have been synthesized,[27] low-pressure chemical-vapor-deposition (CVD) synthesis of large-area few-layer BN doped graphene (BNG) has been presented, leading to BN concentrations as high as 10%; the BN content in BNG layers has been discussed to be related to the heating temperature of the precursor, as confirmed by X-ray photoelectron spectroscopy measurements.[28] The synthesis of a quasi-freestanding BNG monolayer heterostructure, with preferred *zigzag* type boundary, on a weakly coupled Ir-surface has also been recently reported.[29]

In this study we apply *ab initio* quantum-mechanical simulations and show how, by doping graphene with BN inclusions arranged according to different patterns and exploring different substitutional fractions x, a piezoelectricity can be induced in 2D graphene which is found to be 3 to 4 times larger than pure 2D BN monolayer and one order of magnitude larger than previously reported on graphene. Carbon pairs are substituted with BN pairs so as to reduce point symmetry from the centrosymmetric D_{6h} to the non-centrosymmetric D_{3h} group. The full set of piezoelectric constants (elements of the third-order direct, $\mathbf{e}$, and converse, $\mathbf{d}$, piezoelectric tensors) and elastic constants (elements of the fourth-rank elastic, $\mathbb{C}$, and compliance, $\mathbb{S}$, tensors) of all configurations is determined. Both electronic and nuclear-relaxation contributions to the piezoelectric and elastic response of BNG are explicitly taken into account. In the linear regime, direct and converse piezoelectric tensors describe the polarization induced by strain and the strain induced by an external electric field, respectively; a simple connection exists between the two ($\mathbf{e} = \mathbf{d}\,\mathbb{C}$ or $\mathbf{d} = \mathbf{e}\,\mathbb{S}$) via the elastic tensors. Piezoelectric constants can be decomposed into purely electronic "clamped-ion" and nuclear "internal-strain" contributions, where the latter measures the piezoelectric effect due to relaxation of the relative positions of atoms induced by strain[30,31] and is strongly affected by soft phonon modes. Given the high rigidity of graphene, the electronic term is here expected to dominate the response.

2 Computational Approach

The computational scheme we adopt consists in directly computing the intensity of polarization induced by strain, according to the so-called Berry phase approach,[32–34] as implemented[35,36] in the CRYSTAL14 program[37,38] that is here used for all calculations in combination with the hybrid B3LYP functional[39] of the density-functional-theory (DFT) and an atom-centered all-electron basis set of triple-zeta quality, augmented with polarization functions, 6-42111G(*spd*).[40] The level of accuracy in evaluating the Coulomb and exact exchange infinite series is controlled by five thresholds set to T_1=T_2=T_3=T_4=1/2T_5=8.[38] Reciprocal space is sampled according to a regular Pack-Monkhorst sub-lattice with a shrinking factor of 12, corresponding to 19 independent k-points in the first irreducible Brillouin zone of all D_{3h} structures. The present computational setup is the same as that used in a previous investigation on large Carbon nanotubes[41] which led to an accurate description of electronic properties such as the band gap. At variance with the case of polyacetylene (PA),[42] the calculation of the piezoelectric response of BN-doped graphene is not much sensitive to the adopted DFT functional (see comparison with LDA results in Supporting Information). We recently utilized the same approach for investigating the piezoelectric response of 3D systems such as $SrTiO_3$,[35] $BaTiO_3$,[43] Ge-doped quartz[44] and low-dimensional systems such as *h*-BN,[45] *h*-ZnO,[46] and BeO nanotubes.[47] Elastic constants and related properties are computed as strain numerical derivatives of analytical energy gradients.[48–50]

3 Results and Discussion

We consider graphene embedded with periodic arrangements of *zigzag*-edged hexagonal $(BN)_3$ which have recently been shown to be more stable than other arrangements.[51] Different configurations are explored where the size of the BN rings and their separation are changed. In order to unambiguously label each configuration, we adopt a notation first introduced to study graphene antidot lattices and then extended to BNG structures.[52] Each configuration is labeled by a pair of integer indices within brackets, (R,W). R represents the “radius” of the BN rings (measured in

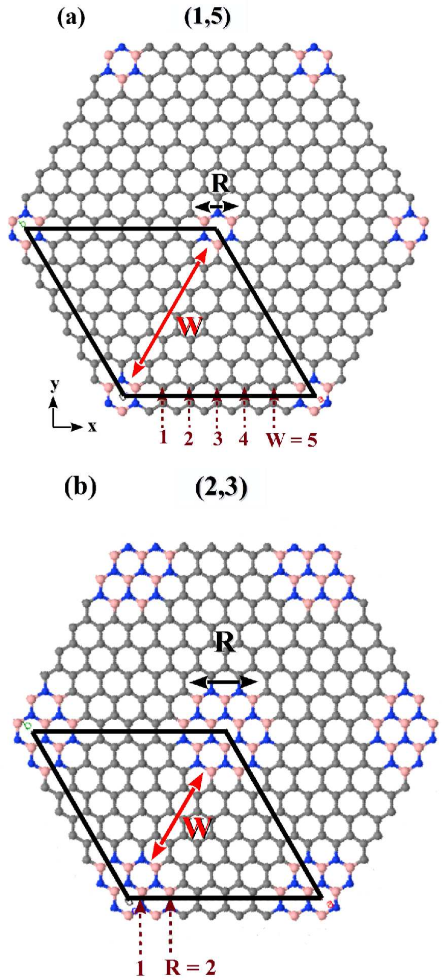

Figure 1: (color online) BN-doped piezoelectric graphene in different configurations (R, W). The radius R of BN rings and the wall width W separating them are graphically defined. The unit cell of each configuration is shown as thick black lines.

units as the number of hexagonal carbon chains substituted with BN atoms) or, equivalently, the number of BN substituted atoms along each of the six sides of the BN hexagons. The separation, or "wall width", between neighboring BNs is represented by the integer W corresponding to the number of non-substituted carbon chains between neighboring BN hexagons. These two indices are graphically defined in Figure 1, where the $(1,5)$ and $(2,3)$ configurations are taken as representatives of two classes of structures with different size. We anticipate that by increasing R (*i.e.* by increasing the substitutional fraction of BN), the piezoelectric response of BNG decreases. The structural parameter that effectively allows for fine-tuning BNG response properties is, indeed, W, as already noticed for the electronic band gap,[52] and for this reason it will be explicitly investigated

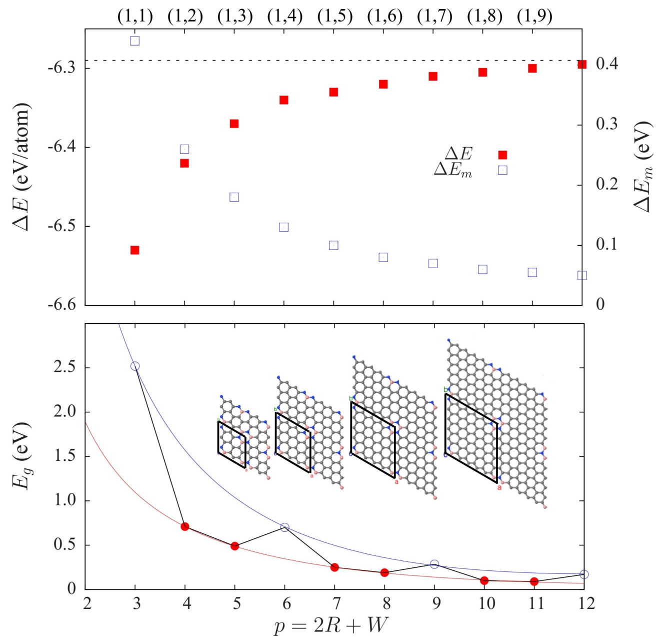

Figure 2: (color online) Energetic and electronic properties of $(1,W)$ BNG structures as a function of $p = 2R+W$. Upper panel: cohesive energy ΔE (the graphene, $p \to \infty$, limit is given by the horizontal line) and energy of mixing ΔE_m (zero by definition at p=0 and p=∞). Lower panel: evolution of the electronic band gap E_g; red and blue lines are just meant as eye-guides. The inset shows the structure of $(1,W)$ BNG configurations as p increases.

in the following discussion.

Before illustrating the dependence on W of the elastic and piezoelectric response of BNG structures, we discuss its effect on energetic and electronic properties, such as the cohesive energy ΔE, the energy of mixing ΔE_m and the electronic band gap E_g. All these quantities are reported, for a series of $(1,W)$ BNG structures, in the two panels of Figure 2 as a function of an integer index $p = 2R+W$ which measures the length of the lattice parameters (kept equal to each other) in units of the total number of atomic C-C chains contained in the unit cell (see Figure 1 for a graphical interpretation of this index). Note that p is related to the BN substitutional fraction x according to $x = 3/p^2$ for $(1,W)$ BNG series. This relation can easily be understood by referring, for instance, to the two panels of Figure 1, where it is seen that the unit cell contains a total of $2p^2$ atoms, out of which $6 \times R^2$ are BN-substituted. This gives a substitutional fraction $x = 6 \times R^2/2p^2$, which reduces to $x = 3/p^2$ when $R = 1$. The inset of the lower panel of the figure shows the effect of increasing the "wall width" W on the structure of BNG and on the size of the corresponding unit cell for R=1. The cohesive energy of each BNG structure (solid red squares in the upper panel of the figure) is defined as: $\Delta E = (E_{\mathrm{BNG}} - N_{\mathrm{B}}E_{\mathrm{B}} - N_{\mathrm{N}}E_{\mathrm{N}} - N_{\mathrm{C}}E_{\mathrm{C}})/(N_{\mathrm{B}} + N_{\mathrm{N}} + N_{\mathrm{C}})$, where E_{BNG} is the energy per unit cell of the BNG configuration, E_{B}, E_{N} and E_{C} the energies of free B, N and C atoms, and N_{B}, N_{N} and N_{C} the number of B, N and C atoms per unit cell. The cohesive energy of pristine *h*-BN is -7.66 eV/atom and remains negative for all BNG structures as a function of p, thus reflecting their strong stability. As p increases (*i.e.* as the BN concentration decreases), ΔE regularly tends to the pristine graphene limit of -6.29 eV/atom (represented as a horizontal dashed line in the figure). The energy of mixing of a $(\mathrm{BN})_x\mathrm{G}_{1-x}$ structure, with x substitutional fraction of BN for carbon pairs, $\Delta E_m = E_{(\mathrm{BN})_x\mathrm{G}_{1-x}} - [xE_{\mathrm{BN}} + (1-x)E_{\mathrm{G}}]$, is a measure of how favorable the formation of a BNG structure is with respect to isolated pristine *h*-BN and graphene. Static computed values are reported, as empty blue squares in the upper panel of Figure 2. Given that entropic thermal terms are not explicitly accounted, they are always positive but rather small, the maximum value being 0.44 eV for the (1,1) case (*i.e.* p=3, x=0.3$\overline{3}$). ΔE_m then progressively decreases as a function of p; according to this merely electronic picture, BN-doped graphene is predicted to be more stable than carbon-doped *h*-BN with respect to the separate phases of *h*-BN and graphene.

The computed value of the band gap of pristine *h*-BN is here 6.73 eV with experimental values usually found in the relatively wide range $4.6 < E_g \leq 7$ eV.[53,54] Electronic energy gaps of $(1,W)$ BNG structures are reported as a function of p in the lower panel of Figure 2. Different symbols are used for cases where p is a multiple of 3 (empty blue circles) and where it is not (full red circles). Overall, the band gap decreases as the concentration of BN decreases, as expected, but with different steepness in the two cases so that the dependence of E_g on p appears to be oscillating, where it appears to be linear with respect to BN concentration x by separating the two p cases (see Figure S1 in Supporting Information). The different behavior of these two classes (multiples of 3 or not of the primitive cell of the pristine system) of graphene superlattices is now well-understood in terms of the energy band-folding model.[55–57] Indeed, even in pure graphene, when p is a multiple of 3, the two Dirac points K and K$'$ in the primitive cell are folded to the Γ point

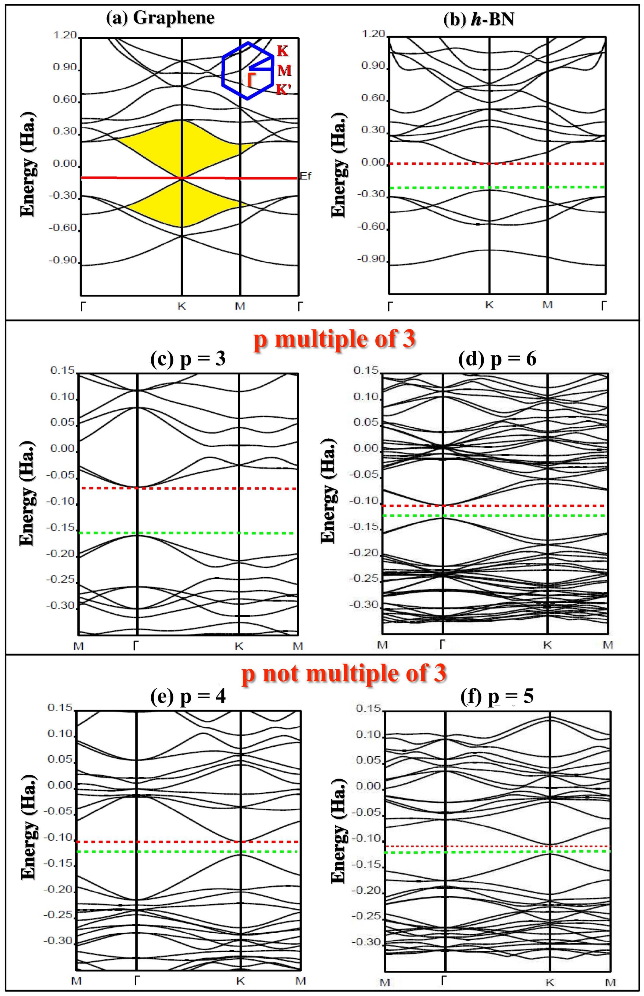

Figure 3: (color online) Energy band structure of (a) pristine graphene, (b) pristine *h*-BN, (c-d) BNG $(1,W)$ structures with p multiple of 3, (e-f) BNG $(1,W)$ structures with p not multiple of 3. HOCO and LUCO energy levels are drawn as dashed green and red lines, respectively.

of the hexagonal first-Brillouin zone (BZ) of the superlattice, giving rise to a fourfold degeneracy that can be broken, opening a band gap, by a periodic arrangement of defects. In the other case, the twofold degenerate Dirac points do not fold into Γ and a band gap opening can be induced by breaking the inversion symmetry.[55] We will discuss below how these two cases can be clearly discriminated also from the analysis of the elastic and piezoelectric response of BNG structures. Band structures of pristine graphene and *h*-BN, and $(1,W)$ BNG structures with different BN concentrations (*i.e.* different p values) are reported in Figure 3. Panels (a) and (b) clearly show the occurrence of a zero and non-zero band gap in graphene and *h*-BN, respectively, at point K of the BZ (schematically represented in blue lines). The area of Dirac conical intersection between valence and conduction bands in graphene is highlighted in yellow whereas the highest occupied (HOCO) and lowest unoccupied (LUCO) crystalline orbital energy levels are represented as dashed green and red lines, respectively. Panels (c) and (d) clearly show the opening of a direct band gap E_g at the Γ point for BNG configurations with p multiple of 3 (p=3 corresponding to a (1,1) and p=6 to a (1,4) structure). On the contrary, panels (e) and (f) show how the direct band gap E_g for cases where p is not a multiple of 3 (p=4 and p=5 corresponding to (1,2) and (1,3) structures) is opened at the K point of the BZ. Again, it is clearly seen that, as p increases, E_g systematically decreases.

Direct and converse piezoelectric tensors are connected via elastic stiffness and compliance tensors; for this reason, before illustrating the piezoelectric response of BNG structures, let us discuss their elastic behavior. According to Voigt's notation,[58] the elastic tensor $\mathbb{C}$ of a 2D system can be represented in terms of a 3×3 matrix whose elements (*i.e.* the elastic stiffness constants) are defined as $C_{vu} = 1/S[\partial^2 E/(\partial\eta_v\partial\eta_u)]$ where S is the area of the 2D cell, E the total energy per cell, η is the strain tensor and $v, u = 1, 2, 6$ (1=xx, 2=yy and 6=xy). The compliance tensor is simply obtained by inverting the stiffness tensor: $\mathbb{S} = \mathbb{C}^{-1}$. Given their symmetry invariance with respect to all the operators of the point group of the system, both tensors exhibit just two symmetry-independent constants: C_{11}, C_{12} and S_{11}, S_{12}. From the knowledge of the full elastic tensor, a number of elastic properties can be derived, such as bulk, shear and Young's moduli, Poisson's ratio, seismic wave velocities, etc.[48,50,58,59] For 2D systems, the Young's modulus is given by $Y_S = (C_{11}^2 - C_{12}^2)/C_{11}$, Poisson's ratio by $\nu = C_{12}/C_{11}$ and bulk modulus by $K_S = (C_{11} + C_{12})/2$ and corresponds to $K_S = S(\partial^2 E/\partial S^2)$.

All these quantities are given in Table 1 for pristine graphene and h-BN, and for $(BN)_x G_{1-x}$ structures of intermediate compositions: from (1,1) where x=0.3$\overline{3}$ to (1,8) where x=0.03. Total values are reported along with nuclear relaxation contributions (in parentheses). Few elastic properties have been experimentally determined for graphene by nanoindentation in an atomic force microscope: its C_{11} stiffness constant and its Young's modulus.[60] Computed counterparts do agree with

Table 1: Elastic properties of $(BN)_xG_{1-x}$ structures in the whole composition range. Elastic stiffness constants, C_{vu}, Young's modulus, Y_S, and bulk modulus, K_S, are given in N/m. Compliance constants, S_{vu}, are given in 10^{-3} m/N while Poisson's ratio, ν, is dimensionless. Total values are reported along with purely nuclear relaxation effects (in parentheses).

	C_{11}	C_{12}	S_{11}	S_{12}	Y_S	K_S	ν
$G_{Exp.}$ [60]	340±50				335±33		
G	372.34	69.47	2.78	-0.52	359.38	220.91	0.187
	(-6.56)	(6.01)	(0.06)	(-0.07)	(-8.89)	(-0.28)	(0.019)
(1,8)	371.30	67.06	2.78	-0.50	359.19	219.18	0.181
	(-7.22)	(6.43)	(0.07)	(-0.07)	(-9.62)	(-0.39)	(0.020)
(1,7)	371.40	66.17	2.78	-0.50	359.61	218.79	0.178
	(-7.69)	(6.79)	(0.08)	(-0.08)	(-10.18)	(-0.45)	(0.022)
(1,6)	369.60	66.97	2.80	-0.51	357.47	218.29	0.181
	(-7.49)	(6.52)	(0.08)	(-0.07)	(-9.93)	(-0.48)	(0.021)
(1,5)	368.22	66.82	2.81	-0.51	356.09	217.52	0.181
	(-7.70)	(6.58)	(0.08)	(-0.07)	(-10.17)	(-0.56)	(0.021)
(1,4)	367.52	64.91	2.81	-0.50	356.06	216.22	0.177
	(-9.40)	(7.47)	(0.09)	(-0.09)	(-11.74)	(-0.79)	(0.024)
(1,3)	362.40	66.39	2.86	-0.52	350.24	214.40	0.183
	(-8.41)	(6.80)	(0.09)	(-0.08)	(-11.00)	(-0.81)	(0.022)
(1,2)	355.89	65.77	2.91	-0.54	343.74	210.83	0.185
	(-9.20)	(6.94)	(0.10)	(-0.09)	(-11.87)	(-1.13)	(0.024)
(1,1)	343.10	61.00	3.01	-0.54	332.25	202.04	0.178
	(-13.29)	(8.15)	(0.14)	(-0.11)	(-16.30)	(-2.57)	(0.029)
h-BN	306.39	64.26	3.41	-0.72	292.91	185.33	0.210
	(-9.92)	(9.65)	(0.15)	(-0.16)	(-13.97)	(-0.14)	(0.037)

these determinations, particularly so as regards their relative values, C_{11} being slightly larger than Y_S. So far, no experimental determinations of such properties have been reported for free-standing monolayer *h*-BN. Previous DFT calculations report K_S values of 160 N/m with local-density[61] (LDA) and 179 N/m with generalized-gradient[59] (PBE) approximations. Our computed value, at B3LYP hybrid level, is 185.3 N/m with a Poisson's ratio ν=0.210 which measures the induced deformation orthogonally to the applied strain and nicely compares with a previous determination of 0.218.[59] As regards intermediate compositions, a rather regular trend is observed in passing from *h*-BN to pure graphene for all elastic properties, again with some oscillations corresponding

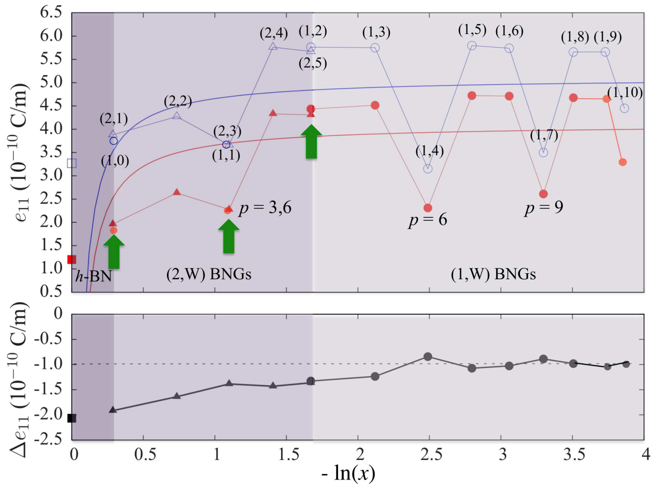

Figure 4: (color online) Upper panel: direct piezoelectric constant e_{11} of BNG structures as a function of -ln(x) where x is the BN substitution fraction; total (full symbols) and purely electronic (empty symbols) values are reported for $(1,W)$ BNGs (circles), $(2,W)$ BNGs (triangles) and pure h-BN (squares). Purely electronic and total data are fitted with a function $a+b/(-\ln(x))$. Lower panel: nuclear relaxation effect on the e_{11} piezoelectric constant, $\Delta e_{11} = e_{11}^{\text{tot}} - e_{11}^{\text{ele}}$ as a function of -ln(x).

to BNG structures with p multiple of 3, such as (1,1), (1,4) and (1,7). The nuclear relaxation effect is seen to be quite small in all cases if compared with the electronic one: it never counts more than 3.8% for the dominant C_{11} constant, which occurs for the (1,1) BNG structure of highest BN concentration. Then, it rapidly decreases to about 2% for BN concentrations below 5% and it remains almost constant down to pristine graphene where it amounts to 1.8%. An analogous behavior is observed also for the compliance constants. The vibrational contribution in pure graphene can be interpreted by considering the elastic deformation as a movement of carbon atoms in collective modes. This movement would lead to a polarization change which, however, is canceled by the inversion symmetry center of D_{6h} graphene, as we will mention below.

Pristine graphene, belonging to the D_{6h} symmetry point group, exhibits an inversion center which prevents it to be piezoelectric. BNG structures are here considered with periodic arrangements of BN domains which break such an inversion and reduce the symmetry to D_{3h}, a point group that enables a piezoelectric response. A Berry-phase approach is adopted that computes the direct piezoelectric constants e_{iv} where $i = x,y$ represents the in-plane Cartesian component of the polarization and v is an index representing the applied strain in Voigt's notation. Given the D_{3h}

symmetry, a single constant is enough for describing the whole in-plane anisotropic piezoelectric response of BNG structures: $e_{11} = -e_{12} = -e_{26}$, the other constants being null by symmetry. The converse piezoelectric effect (represented by the d_{11} constant) is then described by coupling the direct one with the compliance response. For this reason, we discuss the effect of different BN patterns and concentrations, and of the nuclear relaxation, on the direct e_{11} constant (see Figure 4). In the upper panel, the direct piezoelectric constant is reported as a function of BN doping concentration x, as obtained by including (full symbols) or not (empty symbols) the nuclear relaxation effect, for pure h-BN (squares), $(2,W)$ BNGs (triangles) and $(1,W)$ BNGs (circles). We notice that: (i) the computed value of e_{11} for pure h-BN, 1.20×10^{-10} C/m, is remarkably close to a previous theoretical determination: 1.19×10^{-10} C/m;[62] (ii) as discussed for the electronic band gap E_g, at relatively high BN concentrations, the electronic term of the piezoelectric response shows two distinct behaviors depending on p being or not a multiple of 3; (iii) the two different BN patterns provide an almost identical piezoelectric response as a function of BN concentration x (see the green arrows in the figure that mark compositions where $(1,W)$ and $(2,W)$ give exactly the same piezoelectric response). In the lower panel of the figure, the nuclear relaxation contribution is reported. We see that: (i) it systematically reduces the purely electronic piezoelectric response; (ii) it is rather large for pristine h-BN (-2.1×10^{-10} C/m, corresponding to 60% of the electronic term), it progressively reduces as the BN concentration decreases and it becomes practically constant as x becomes lower than 10% (about -1.0×10^{-10} C/m, corresponding to just 20% and 16% of the electronic contribution for p multiple or not of 3, respectively). The same trend has already been discussed for elasticity. An explanation for such a behavior can be demonstrated as due to soft (low-frequency) collective modes of small infrared (IR) intensity (see Supporting Information, Figure S2: the IR spectrum of large BNG supercells). Another important finding, represented in Figure 4, is that, for BN concentrations below about 33%, the piezoelectric response of BN-doped graphene is found to be essentially constant for p not multiple of 3, rapidly converging to the limit value of about 4.5×10^{-10} C/m as x decreases. For p multiple of 3, the convergence is slower and still not completely reached at $p = 12$ (the purely electronic contribution to e_{11} still

Table 2: Direct and converse piezoelectric constants of BN-doped graphene (at infinite defect dilution) as computed in the present study and as compared to experimental and theoretical values of other 2D and 3D piezoelectric materials. Direct e constants are reported in 10^{-10}C/m for 2D system and in C/m^2 for 3D system. Converse d constants are expressed in pm/V.

System	e	d
BN-doped Graphene (This study)	4.5 (e_{11})	1.5 (d_{11})
h-BN (This study)	1.2 (e_{11})	0.5 (d_{11})
Graphene + Li[20]	0.5 (e_{31})	0.1 (d_{31})
h-BN + F,H (chair)[63]	1.8 (e_{11})	1.3 (d_{11})
h-MoS_2[64]	2.9 (e_{11})	-
Bulk α-Quartz[65]	0.2 (e_{11})	2.3 (d_{11})
$Si_{0.83}Ge_{0.16}O_2$[44]	0.2 (e_{11})	5.5 (d_{11})
Bulk GaN[66]	1.1 (e_{33})	3.7 (d_{33})
Bulk AlN[66]	1.5 (e_{33})	5.6 (d_{33})

increases to 4.45×10^{-10} C/m). However, the same piezoelectricity value as the converged one for the p not multiple of 3 series should be obtained at the $p \rightarrow \infty$ limit (*i.e.* the piezoelectricity value of inversion symmetry-broken graphene). A fit of purely electronic contributions leads to a limit value of about 5.5×10^{-10} C/m at infinite BN dilution which would imply a corresponding value of approximatively 4.5×10^{-10} C/m for the total piezoelectricity. The finite and constant piezoelectric response of D_{3h} graphene at infinite defect dilution can be explained as follows: as the BN concentration decreases, on the one hand the narrowing of the electronic band gap E_g would lead to an infinite piezoelectric response whereas, on the other hand the reduction of the degree of symmetry inversion breaking with respect to pure graphene would lead to a zero piezoelectricity. As a result of the balance between these two limits, BNG structures are found to exhibit a non-null, non-infinite, constant piezoelectric response. Both compensating effects (*i.e.* vanishing band gap and recovering of inversion symmetry) are essentially intrinsic of graphene and do not depend on the particular physical or chemical nature of the inversion symmetry breaking defects, as we demonstrate in Supporting Information and as we will explicitly show below by considering graphene with different patterns of D_{3h} and C_{2v} holes.

Before discussing the effect of other types of inversion symmetry breaking defects on the piezoelectricity of graphene, let us discuss the magnitude of the piezoelectric response of BN-doped graphene by comparing with typical values of piezoelectric constants of other 2D and 3D systems. In Table 2, we report our computed values for the e_{11} and d_{11} piezoelectric constants of pristine h-BN and BN-doped graphene (in the limit of vanishing defect concentration) along with experimental and theoretical determinations of the highest piezoelectric constants of other materials. It is seen that the piezoelectricity induced in graphene by BN symmetry breaking is one order of magnitude larger than the largest one, corresponding to the e_{31} constant, that could be induced by adsorbing Li atoms on its surface, due to the fact that an out-of-plane, instead of an in-plane, polarization was generated in that case.[20] BN-induced direct piezoelectricity in graphene is almost 4 times larger than that of pristine h-BN, more than twice the maximum one predicted for F- and H-doped h-BN in a chair conformation[63] and 60% larger than the experimentally measured one for the h-MoS_2 monolayer.[64] When comparing with 3D systems, we notice that the converse piezoelectric constant d_{11} of BNG structures (in pm/V) is of the same order of magnitude but systematically smaller than those of bulk quartz, GaN and AlN, for instance. In order to compare present values of the direct piezoelectric response of the monolayers with those of standard 3D piezoelectric materials, we need to define a volume and to consider, as it is generally done in these cases, a graphite-like system with interlayer distance[67] of 3.35 Å. It follows that BNG structures exhibit a direct macroscopic piezoelectricity that is about 10 times larger than that of pure α-quartz[65] or Ge-doped α-quartz,[44] 5 times larger than that (0.27 C/m^2) of polyvinylidene fluoride and its copolymers[68] and comparable to that of bulk GaN and AlN.[66]

In order to confirm that the same finite, large, piezoelectric response can be induced in graphene simply by breaking its inversion symmetry center with **any** in-plane defect, in the limit of low defect concentration, we introduce two other defects: holes which reduce the symmetry of graphene from D_{6h} to D_{3h} and C_{2v}, respectively. A graphical representation of the resulting structure of the perturbed graphene sheet in the two cases is given in Figure 5. For each type of hole, a series of structures corresponding to different defect concentrations are considered for which the purely

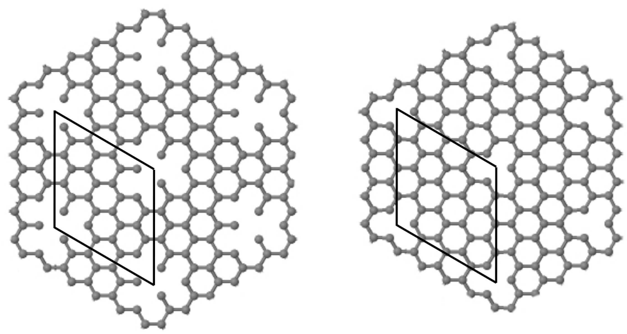

Figure 5: (color online) Graphical representation of the structure of two defects, one of D_{3h} and one of C_{2v} point-symmetry, of graphene (holes in this case) that break its inversion symmetry. The unit cell of the p=4 case is sketched in both cases with black continuous lines.

electronic contribution of the in-plane piezoelectric response, e_{11}^{ele} constant, is evaluated. These results are reported in Figure 6 along with the corresponding ones of the two series of $(1,W)$ and $(2,W)$ BN-doped structures. From the analysis of the figure, it turns out that, although with different steepness and behaviors, all defects induce a large piezoelectric response in graphene essentially converging to the same value as the dilution of the defects increases. For the two most regularly converging series ($(1,W)$ BNGs and D_{3h} holes), a fitting $a+b/(-\ln(x))$ is reported which highlights the common piezoelectric response in the limit of low defect concentration. The piezoelectricity value of each largest supercell system is found in the range: e_{11}^{ele}=5.6±0.4×10^{-10} C/m.

The present results on graphene holes do apparently contradict those of a recent investigation of the piezoelectric response of graphene with triangular holes where a very low piezoelectricity (0.124 C/m^2) was reported.[69] However, in that study, performed with a plane-wave periodic program, the graphene layer was described in terms of a 3D model with a very large unit cell of non-interacting repeated layers and the results, given in units of a 3D system, were wrongly divided by the 3D cell volume thus resulting in an apparent very low piezoelectric response.

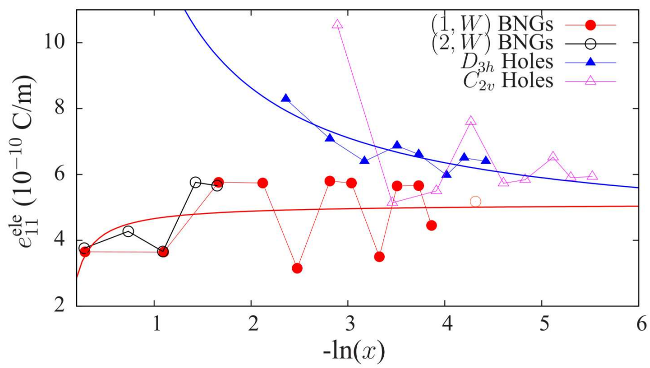

Figure 6: (color online) Dependence of the in-plane direct piezoelectric constant of graphene, e_{11}^{ele} (purely electronic contribution), on defect concentration x. Four different defects are considered: $(1,W)$ BNGs (full red circles), $(2,W)$ BNGs (empty black circles), D_{3h} holes (full blue triangles) and C_{2v} holes (empty magenta triangles). For $(1,W)$ BNGs and D_{3h} holes the fitting $a+b/(-\ln(x))$ is also reported. All results are obtained at the B3LYP level. For $(1,W)$ BNGs, a LDA result is also shown (red empty circle) at lower defect concentration.

4 Conclusions

It has been shown as a large in-plane piezoelectricity (one order of magnitude larger than the out-of-plane one previously reported) can be induced in graphene by including in-plane defects that reduce its point symmetry from D_{6h} to either D_{3h} or C_{2v}. Different patterns and concentrations of periodically-arranged BN domains and holes have been considered. Direct and converse piezoelectricity is shown to be dominated by the electronic contribution, and to tend towards a unique value, neither null nor infinite, in the limit of pure symmetry-broken graphene. This behavior could have a significant technological impact in the practical fabrication of NEMS devices.

Acknowledgements The authors gratefully acknowledge the Centre Informatique National de l'Enseignement Supérieur (CINES) for computing facilities. El-Kelany acknowledges the Egyptian government for supporting with a grant his work at the Université de Pau et des Pays de l'Adour in France. Discussions with Dr. Panos Karamanis are gratefully acknowledged.

Supporting Information Available The interpretation of piezoelectricity as a second-order energy perturbation. The linear behavior of the electronic band gap of $(1,W)$ BNG structures as a function of BN concentration. The evidence of the consistency of vibrational contributions to the piezoelectricity and to the IR intensity of soft (low-frequency) collective modes. The independence of piezoelectricity from DFT functional. This material is available free of charge at http://pubs.acs.org

References

(1) Craighead, H. G. Nanoelectromechanical Systems. *Science* **2000**, *290*, 1532–1535.

(2) Ekinci, K. L.; Roukes, M. L. Nanoelectromechanical Systems. *Review of Scientific Instruments* **2005**, *76*, 061101.

(3) Henry Huang, X. M.; Zorman, C. A.; Mehregany, M.; Roukes, M. L. Nanoelectromechanical Systems: Nanodevice Motion at Microwave Frequencies. *Nature* **2003**, *421*, 496–496.

(4) Wang, X.; Song, J.; Zhang, F.; He, C.; Hu, Z.; Wang, Z. Electricity Generation Based on One-Dimensional Group-III Nitride Nanomaterials. *Adv. Mater.* **2010**, *22*, 2155–2158.

(5) Nechibvute, A.; Chawanda, A.; Luhanga, P. Piezoelectric Energy Harvesting Devices: An Alternative Energy Source for Wireless Sensors. *Smart Materials Research* **2012**, *2012*, 853481.

(6) Madden, J. D.; Vandesteeg, N. A.; Anquetil, P. A.; Madden, P. G.; Takshi, A.; Pytel, R. Z.; Lafontaine, S. R.; Wieringa, P. A.; Hunter, I. W. Artificial Muscle Technology: Physical Principles and Naval Prospects. *IEEE J. Oceanic Eng.* **2004**, *29*, 706–728.

(7) Gautschi, G. *Piezoelectric Sensorics: Force, Strain, Pressure, Acceleration and Acoustic Emission Sensors, Materials and Amplifiers*; Engineering online library; Springer, 2002.

(8) Wang, Y.; Herron, N. Nanometer-Sized Semiconductor Clusters: Materials Synthesis, Quantum Size Effects, and Photophysical Properties. *J. Phys. Chem.* **1991**, *95*, 525–532.

(9) Novoselov, K. S.; Geim, A. K.; Morozov, S. V.; Jiang, D.; Zhang, Y.; Dubonos, S. V.; Grigorieva, I. V.; Firsov, A. A. Electric Field Effect in Atomically Thin Carbon Films. *Science* **2004**, *306*, 666–669.

(10) Novoselov, K. S.; Geim, A. K.; Morozov, S. V.; Jiang, D.; Katsnelson, M. I.; Grigorieva, I. V.; Dubonos, S. V.; Firsov, A. A. Two-Dimensional Gas of Massless Dirac Fermions in Graphene. *Nature* **2005**, *438*, 197–200.

(11) Bolotin, K. I.; Ghahari, F.; Shulman, M. D.; Stormer, H. L.; Kim, P. Observation of the Fractional Quantum Hall Effect in Graphene. *Nature* **2009**, *462*, 196–199.

(12) Cheng, R.; Bai, J.; Liao, L.; Zhou, H.; Chen, Y.; Liu, L.; Lin, Y.-C.; Jiang, S.; Huang, Y.; Duan, X. High-frequency Self-Aligned Graphene Transistors with Transferred Gate Stacks. *Proc. Nat. Acad. Sci.* **2012**, *109*, 11588–11592.

(13) Wu, Y.; Jenkins, K. A.; Valdes-Garcia, A.; Farmer, D. B.; Zhu, Y.; Bol, A. A.; Dimitrakopoulos, C.; Zhu, W.; Xia, F.; Avouris, P.; Lin, Y.-M. State-of-the-Art Graphene High-Frequency Electronics. *Nano Lett.* **2012**, *12*, 3062–3067.

(14) Bonaccorso, F.; Sun, Z.; Hasan, T.; Ferrari, A. C. Graphene Photonics and Optoelectronics. *Nat. Photon.* **2010**, *4*, 611–622.

(15) Dlubak, B.; Martin, M.-B.; Deranlot, C.; Servet, B.; Xavier, S.; Mattana, R.; Sprinkle, M.; Berger, C.; De Heer, W. A.; Petroff, F.; Anane, A.; Seneor, P.; Fert, A. Highly Efficient Spin Transport in Epitaxial Graphene on SiC. *Nat. Phys.* **2012**, *8*, 557–661.

(16) Kou, L.; Tang, C.; Chen, C.; Guo, W. Hybrid W-shaped Graphene Nanoribbons: Distinct Electronic and Transport Properties. *J. Appl. Phys.* **2011**, *110*, 124312.

(17) Geim, A. K.; Novoselov, K. S. The Rise of Graphene. *Nat. Mater.* **2007**, *6*, 183–191.

(18) Castro Neto, A. H.; Guinea, F.; Peres, N. M. R.; Novoselov, K. S.; Geim, A. K. The Electronic Properties of Graphene. *Rev. Mod. Phys.* **2009**, *81*, 109–162.

(19) Allen, M. J.; Tung, V. C.; Kaner, R. B. Honeycomb Carbon: A Review of Graphene. *Chemical Reviews* **2010**, *110*, 132–145.

(20) Ong, M. T.; Reed, E. J. Engineered Piezoelectricity in Graphene. *ACS Nano* **2012**, *6*, 1387–1394.

(21) De La Pierre, M.; Karamanis, P.; Baima, J.; Orlando, R.; Pouchan, C.; Dovesi, R. Ab initio Periodic Simulation of the Spectroscopic and Optical Properties of Novel Porous Graphene Phases. *J. Phys. Chem. C* **2013**, *117*, 2222–2229.

(22) Zhang, Y.; Tang, T.-T.; Girit, C.; Hao, Z.; Martin, M.; Zettl, A.; Crommie, M. F.; Shen, Y. R.; Wang, F. Direct Observation of a Widely Tunable Bandgap in Bilayer Graphene. *Nature* **2009**, *459*, 820–823.

(23) Naumov, I. I.; Bratkovsky, A. M. Gap Opening in Graphene by Simple Periodic Inhomogeneous Strain. *Phys. Rev. B* **2011**, *84*, 245444.

(24) Shi, Y.; Kim, K. K.; Reina, A.; Hofmann, M.; Li, L.-J.; Kong, J. Work Function Engineering of Graphene Electrode via Chemical Doping. *ACS Nano* **2010**, *4*, 2689–2694, PMID: 20433163.

(25) Usachov, D.; Vilkov, O.; Grüneis, A.; Haberer, D.; Fedorov, A.; Adamchuk, V. K.; Preobrajenski, A. B.; Dudin, P.; Barinov, A.; Oehzelt, M.; Laubschat, C.; Vyalikh, D. V. Nitrogen-Doped Graphene: Efficient Growth, Structure, and Electronic Properties. *Nano Lett.* **2011**, *11*, 5401–5407.

(26) Karamanis, P.; Otero, N.; Pouchan, C. Unleashing the Quadratic Nonlinear Optical Responses of Graphene by Confining White-Graphene (h-BN) Sections in Its Framework. *J. Am. Chem. Soc.* **2014**, *136*, 7464–7473.

(27) Ci, L.; Song, L.; Jin, C.; Jariwala, D.; Wu, D.; Li, Y.; Srivastava, A.; Wang, Z. F.; Storr, K.;

Balicas, L.; Liu, F.; Ajayan, P. M. Atomic Layers of Hybridized Boron Nitride and Graphene Domains. *Nat. Mater.* **2010**, *9*, 430–435.

(28) Chang, C.-K. et al. Band Gap Engineering of Chemical Vapor Deposited Graphene by in Situ BN Doping. *ACS Nano* **2013**, *7*, 1333–1341.

(29) Liu, M.; Li, Y.; Chen, P.; Sun, J.; Ma, D.; Li, Q.; Gao, T.; Gao, Y.; Cheng, Z.; Qiu, X.; Fang, Y.; Zhang, Y.; Liu, Z. Quasi-Freestanding Monolayer Heterostructure of Graphene and Hexagonal Boron Nitride on Ir(111) with a Zigzag Boundary. *Nano Lett.* **2014**, *14*, 6342–6347.

(30) Sághi-Szabó, G.; Cohen, R. E.; Krakauer, H. First-Principles Study of Piezoelectricity in $PbTiO_3$. *Phys. Rev. Lett.* **1998**, *80*, 4321–4324.

(31) Dal Corso, A.; Posternak, M.; Resta, R.; Baldereschi, A. Ab initio Study of Piezoelectricity and Spontaneous Polarization in ZnO. *Phys. Rev. B* **1994**, *50*, 10715–10721.

(32) King-Smith, R. D.; Vanderbilt, D. Theory of Polarization of Crystalline Solids. *Phys. Rev. B* **1993**, *47*, 1651–1654.

(33) Vanderbilt, D. Berry-Phase Theory of Proper Piezoelectric Response. *J. Phys. Chem. Solids* **2000**, *61*, 147–151.

(34) Resta, R. Macroscopic Polarization in Crystalline Dielectrics: the Geometric Phase Approach. *Rev. Mod. Phys.* **1994**, *66*, 899–915.

(35) Erba, A.; El-Kelany, K. E.; Ferrero, M.; Baraille, I.; Rérat, M. Piezoelectricity of $SrTiO_3$: An Ab initio Description. *Phys. Rev. B* **2013**, *88*, 035102.

(36) Noël, Y.; Zicovich-Wilson, C. M.; Civalleri, B.; D'Arco, P.; Dovesi, R. Polarization Properties of ZnO and BeO: An Ab initio Study Through the Berry Phase and Wannier Functions Approaches. *Phys. Rev. B* **2001**, *65*, 014111.

(37) Dovesi, R.; Orlando, R.; Erba, A.; Zicovich-Wilson, C. M.; Civalleri, B.; Casassa, S.; Maschio, L.; Ferrabone, M.; De La Pierre, M.; D'Arco, Ph.; Noël, Y.; Causá, M.; Rérat, M.; Kirtman, B. CRYSTAL14: A Program for the Ab initio Investigation of Crystalline Solids. *Int. J. Quantum Chem.* **2014**, *114*, 1287–1317.

(38) Dovesi, R.; Saunders, V. R.; Roetti, C.; Orlando, R.; Zicovich-Wilson, C. M.; Pascale, F.; Doll, K.; Harrison, N. M.; Civalleri, B.; Bush, I. J.; D'Arco, P.; Llunell, M.; Causà, M.; Noël, Y. CRYSTAL14 User's Manual. 2013; http://www.crystal.unito.it.

(39) Becke, A. D. Density-Functional Exchange-Energy Approximation with Correct Asymptotic Behavior. *Phys. Rev. A* **1988**, *38*, 3098–3100.

(40) Peintinger, M. F.; Oliveira, D. V.; Bredow, T. Consistent Gaussian Basis Sets of Triple-Zeta Valence with Polarization Quality for Solid-State Calculations. *J. Comp. Chem.* **2013**, *34*, 451–459.

(41) Demichelis, R.; Noël, Y.; D'Arco, P.; Rérat, M.; Zicovich-Wilson, C. M.; Dovesi, R. Properties of Carbon Nanotubes: An Ab initio Study Using Large Gaussian Basis Sets and Various DFT Functionals. *J. Phys. Chem. C* **2011**, *115*, 8876–8885.

(42) Lacivita, V.; Rérat, M.; Orlando, R.; Ferrero, M.; Dovesi, R. Calculation of Longitudinal Polarizability and Second Hyperpolarizability of Polyacetylene with the Coupled Perturbed Hartree-Fock/Kohn-Sham Scheme. Where it is Shown how Finite Oligomer Chains Tend to the Infinite Periodic Polymer. *J. Chem. Phys.* **2012**, *136*, 114101.

(43) Mahmoud, A.; Erba, A.; El-Kelany, K. E.; Rérat, M.; Orlando, R. Low-Temperature Phase of $BaTiO_3$: Piezoelectric, Dielectric, Elastic, and Photo-elastic Properties from Ab initio Simulations. *Phys. Rev. B* **2014**, *89*, 045103.

(44) El-Kelany, K. E.; Erba, A.; Carbonnière, P.; Rérat, M. Piezoelectric, Elastic, Structural and Dielectric Properties of $Si_{1-x}Ge_xO_2$ Solid Solution: a Theoretical Study. *J. Phys.: Cond. Matter* **2014**, *26*, 205401.

(45) Erba, A.; Ferrabone, M.; Baima, J.; Orlando, R.; Rérat, M.; Dovesi, R. The Vibration Properties of the (n,0) Boron Nitride Nanotubes from Ab initio Quantum Chemical Simulations. *J. Chem. Phys.* **2013**, *138*, 054906.

(46) Lacivita, V.; Erba, A.; Noël, Y.; Orlando, R.; D'Arco, Ph.; Dovesi, R. Zinc Oxide Nanotubes: An Ab initio Investigation of Their Structural, Vibrational, Elastic, and Dielectric Properties. *J. Chem. Phys.* **2013**, *138*, 214706.

(47) Baima, J.; Erba, A.; Orlando, R.; Rérat, M.; Dovesi, R. Beryllium Oxide Nanotubes and Their Connection to the Flat Monolayer. *J. Phys. Chem. C* **2013**, *117*, 12864–12872.

(48) Erba, A.; Mahmoud, A.; Orlando, R.; Dovesi, R. Elastic Properties of Six Silicate Garnet End-members from Accurate Ab initio Simulations. *Phys. Chem. Min.* **2014**, *41*, 151–160.

(49) Erba, A.; Mahmoud, A.; Orlando, R.; Dovesi, R. Erratum to: Elastic Properties of Six Silicate Garnet End-members from Accurate Ab initio Simulations. *Phys. Chem. Min.* **2014**, *41*, 161–162.

(50) Tan, J. C.; Civalleri, B.; Erba, A.; Albanese, E. Quantum Mechanical Predictions to Elucidate the Anisotropic Elastic Properties of Zeolitic Imidazolate Frameworks: ZIF-4 vs. ZIF-zni. *CrystEngComm* **2015**, *17*, 375–382.

(51) Fan, X.; Shen, Z.; Liu, A. Q.; Kuo, J.-L. Band Gap Opening of Graphene by Doping Small Boron Nitride Domains. *Nanoscale* **2012**, *4*, 2157–2165.

(52) Zhao, R.; Wang, J.; Yang, M.; Liu, Z.; Liu, Z. BN-Embedded Graphene with a Ubiquitous Gap Opening. *J. Phys. Chem. C* **2012**, *116*, 21098–21103.

(53) Nagashima, A.; Tejima, N.; Gamou, Y.; Kawai, T.; Oshima, C. Electronic Dispersion Relations of Monolayer Hexagonal Boron Nitride Formed on the Ni(111) Surface. *Phys. Rev. B* **1995**, *51*, 4606–4613.

(54) Berseneva, N.; Gulans, A.; Krasheninnikov, A. V.; Nieminen, R. M. Electronic Structure of Boron Nitride Sheets Doped with Carbon from First-Principles Calculations. *Phys. Rev. B* **2013**, *87*, 035404.

(55) Xiu, S. L.; Gong, L.; Wang, V.; Liang, Y. Y.; Chen, G.; Kawazoe, Y. Degenerate Perturbation in Band-Gap Opening of Graphene Superlattice. *J. Phys. Chem. C* **2014**, *118*, 8174–8180.

(56) Lambin, P.; Amara, H.; Ducastelle, F.; Henrard, L. Long-Range Interactions Between Substitutional Nitrogen Dopants in Graphene: Electronic Properties Calculations. *Phys. Rev. B* **2012**, *86*, 045448.

(57) Martinazzo, R.; Casolo, S.; Tantardini, G. F. Symmetry-Induced Band-Gap Opening in Graphene Superlattices. *Phys. Rev. B* **2010**, *81*, 245420.

(58) Nye, J. F. *Physical Properties of Crystals: Their Representation by Tensors and Matrices*; Clarendon Press, 1957.

(59) Peng, Q.; Ji, W.; De, S. Mechanical Properties of the Hexagonal Boron Nitride Monolayer: Ab initio Study. *Comput. Mater. Sci.* **2012**, *56*, 11–17.

(60) Lee, C.; Wei, X.; Kysar, J. W.; Hone, J. Measurement of the Elastic Properties and Intrinsic Strength of Monolayer Graphene. *Science* **2008**, *321*, 385–388.

(61) Nag, A.; Raidongia, K.; Hembram, K. P. S. S.; Datta, R.; Waghmare, U. V.; Rao, C. N. R. Graphene Analogues of BN: Novel Synthesis and Properties. *ACS Nano* **2010**, *4*, 1539–1544.

(62) Michel, K. H.; Verberck, B. Theory of Elastic and Piezoelectric Effects in Two-Dimensional Hexagonal Boron Nitride. *Phys. Rev. B* **2009**, *80*, 224301.

(63) Noor-A-Alam, M.; Kim, H. J.; Shin, Y.-H. Dipolar Polarization and Piezoelectricity of a Hexagonal Boron Nitride Sheet Decorated with Hydrogen and Fluorine. *Phys. Chem. Chem. Phys.* **2014**, *16*, 6575–6582.

(64) Zhu, H.; Wang, Y.; Xiao, J.; Liu, M.; Xiong, S.; Wong, Z. J.; Ye, Z.; Yin, X.; Zhang, X. Observation of Piezoelectricity in Monolayer Molybdenum Disulfide. *ArXiv e-prints* **2014**,

(65) Bechmann, R. Elastic and Piezoelectric Constants of Alpha-Quartz. *Phys. Rev.* **1958**, *110*, 1060–1061.

(66) Guy, I. L.; Muensit, S.; Goldys, E. M. Extensional Piezoelectric Coefficients of Gallium Nitride and Aluminum Nitride. *Appl. Phys. Lett.* **1999**, *75*, 4133–4135.

(67) Bacon, G. E. The Interlayer Spacing of Graphite. *Acta Crystallogr.* **1951**, *4*, 558–561.

(68) Nakhmanson, S. M.; Nardelli, M. B.; Bernholc, J. *Ab initio* Studies of Polarization and Piezoelectricity in Vinylidene Fluoride and BN-Based Polymers. *Phys. Rev. Lett.* **2004**, *92*, 115504.

(69) Chandratre, S.; Sharma, P. Coaxing Graphene to be Piezoelectric. *Appl. Phys. Lett.* **2012**, *100*, 023114.